

# Self-Consistent-Field Analysis of Mixed Polyelectrolyte and Neutral Polymer Brushes

Kevin N. Witte and You-Yeon Won\*

School of Chemical Engineering, Purdue University, West Lafayette, Indiana 47907

Received April 13, 2006; Revised Manuscript Received August 14, 2006

**ABSTRACT:** We present a theoretical study of the phase behavior of mixed brushes composed of charged and noncharged polymers that are mutually incompatible. We derive the self-consistent-field (SCF) equations from the canonical ensemble for a system of polyelectrolyte and uncharged polymers with added salt. Within the saddle point approximation, the modified Edwards Hamiltonian results in expressions for the chemical potential and species density fields in terms of the Green's function propagator and the nonlinear Poisson–Boltzmann equation for the electrostatic potential. These SCF equations were fully numerically analyzed to achieve results that are exact within the assumption of lateral mean field. The two-dimensional phase behavior of the mixed brushes (assuming that the brushes are laterally mobile) was examined using the conventional free energy of mixing analysis. The predictions on the effects of such control variables as the charge content of the polyelectrolyte species, ionic strength of the medium, and the surface grafting density of the chains on the conformation properties and phase behavior of the mixed brushes are presented. The results suggest that an increase in the effective charge on the polyelectrolyte (through variation of either charge content or ionic strength) favors the mixed state, while increasing the grafting density favors phase separation.

## 1. Introduction

Solvated polymers end-grafted to a surface have been the subject of intense theoretical and experimental studies over the past three decades. When the grafting density is high enough so that the mean separation between grafting points is less than the coil dimension of the chains in the unbound state, the chains are stretched away from their unperturbed dimension into a “brush” configuration because of the repulsion between monomers; this repulsion is of osmotic origin in neutral brushes, and chain electrostatic and counterion osmotic pressure effects enhance this repulsion if the polymers are charged. The thermal fluctuation of the chain conformation, however, disfavors the stretched state, and the balance between these two opposing forces (i.e., the effective monomer–monomer repulsion which causes the stretching and the thermal (entropic) resistance to this stretching) determines the conformation of the brush. Understanding the behavior of polymers under the tethered conditions is fundamental to many technological applications of polymer brushes, including colloidal stabilization,<sup>1</sup> membrane surface modification,<sup>2</sup> ion-exchange adsorbents,<sup>3</sup> lubricative coating,<sup>4</sup> and the creation of surfaces with externally tunable properties.<sup>5</sup>

The simplest situations involving homogeneous polymer brushes (i.e., those composed of one polymer component)<sup>1,4,6–25</sup> have been explored in great detail; see refs 1, 4, 6–11, and 25 for detailed discussions on theories for neutral brushes and also refs 12–24 for polyelectrolyte brushes. Considerable attention has also been devoted to mixed brushes containing (at least) two chemically distinct polymers. The types of mixed brushes that have been studied include those composed of either two neutral chain types<sup>26–32</sup> or two oppositely charged chain types.<sup>19</sup> It has been demonstrated that, in mixed brushes, the chemical dissimilarity between component polymers offers a possibility for creating lateral and/or vertical compositional heterogeneities on molecular length scales.<sup>29–31</sup> Also, the asymmetry in the

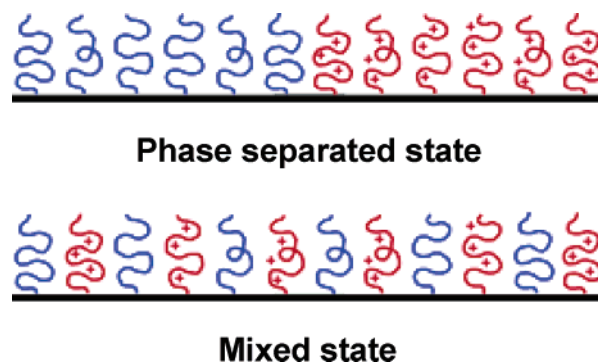


**Figure 1.** Cartoon of macroscopic phase separation in a mixed brush composed of charged (red) and neutral (blue) chains in which the grafting points are laterally mobile. The difference in polymer composition between the phase separated and mixed states is exaggerated for clarity.

responses of the component chains to changes in environmental conditions can be used as a mechanism for creating functional surfaces that are responsive to external stimuli such as variation of pH<sup>19</sup> or electric field.<sup>33</sup>

In all previous studies of mixed brushes, it has been commonly assumed that the chains are chemically bound to the surface, and the positions of the grafting points are fixed in both lateral and vertical directions. However, there are some experimental situations in which the grafted ends in a polymer brush can move on the grafting surface. An important example is when diblock copolymers self-assemble into lamellar structures in selective solvents;<sup>8,34–36</sup> the outer portions of the chains exposed to the solvent will form brush structures in which the grafted ends are mobile along the interfaces formed by the block copolymers. As illustrated in Figure 1, in mixed brushes comprising polymers that are mutually immiscible, this lateral mobility of the end-grafting points has an important consequence of allowing for bulk phase separation between the components within the two-dimensional geometry. Detailed examination of this macroscopic phase segregation that is feasible in end-mobile mixed brushes has not yet been reported to the best of our

\* To whom correspondence should be addressed. E-mail: yywon@ecn.purdue.edu.

knowledge, and this is the topic of this paper. Particularly, the present report presents a theoretical discussion on the miscibility of mixed polymer brushes composed of neutral and polyelectrolyte chains. We note that this type of mixed system has received very little attention in the literature.<sup>19</sup>

The main goal of this work is to examine the macroscopic phase behavior of mixtures of neutral and polyelectrolyte brushes with mobile grafting points in solutions with added salt as a function of charge fraction, added salt concentration, and grafting density. To this end, we employ a self-consistent-field (SCF) theory based on the Edwards model<sup>9,10</sup> and modified to include electrostatic interactions and multiple chain types. Previously, the nonlinear Poisson–Boltzmann (PB) equation (which stipulates the conditions governing the spatial variation of the electric potential in the system) has been handled by either assuming the form of the small ion distribution<sup>23</sup> or linearizing the PB equation.<sup>22</sup> In this work, we solve the PB equation numerically without either assumption. The SCF equations are derived in full starting from the system partition function and ending with equations containing the Edwards–Green’s function as the carrier of the segment probability density. Similar SCF formalisms have been previously utilized for studying polymer adsorption and free polymers in solution; in these cases, rather than the Green’s function, other simpler functions such as Andelman and co-workers’ polymer order parameter<sup>37–39</sup> or Fredrickson and co-workers’  $q$  function<sup>39,40</sup> were employed. In our studies of polyelectrolyte brushes, the polymer order parameter could not have been employed because it does not contain information regarding the chain ends. We chose not to utilize the  $q$  function because the Green’s function contains the chain end information more accessibly. It should also be noted that our approach is consistent with these previous SCF formalisms in that the Green’s function can be simplified to either function by use of the ground state dominance approximation<sup>37–39</sup> or by integrating over the spatial location of the chain ends<sup>39,40</sup> to derive the previous SCF models.

The phase behavior of the polymer brushes is examined by use of phase diagrams containing binodal and spinodal points determined from the free energy of mixing for the two brush types. A detailed derivation of the system free energy from the canonical ensemble partition function is included along with the derivation of the SCF equations. The parameter space near physiological conditions is extensively explored due to an interest in creating biocompatible membranes in future work. Generally, we find that the effective amount of charge in the system has the greatest effect upon the miscibility of the brushes with increasing effective charge favoring greater mixing. This result is consistent with the findings of Khokhlov and Nyrkova that including small amounts of charge on one chain type in a binary polymer mixture greatly increases miscibility.<sup>41</sup>

## 2. Model

**2.1. SCF Formalism.** The SCF formalism is derived, following the development of Wang et al.,<sup>40</sup> by considering homopolymer brushes that may contain charge in solution. The polymers of type  $P$ , either neutral (A) or charged (C), are of length  $N_P$ . The polyelectrolyte chains are assumed to carry a smeared charge with fraction per segment  $f$  and valence  $z_P$  which are identically zero for neutral chains. All small ions, both counterions liberated from the dissociation of the polyelectrolyte and any salt added to the solution, are assumed to be identical point charges with valence  $z_M$ , where  $M$  designates cations (+) or anions (−). In a canonical ensemble with Boltzmann factor  $\beta$  and volume  $V$ , the partition function of the system is

$$Z = \prod_j \frac{1}{n_j!} \prod_P \prod_i^{n_P} \int d\mathbf{R}_{P_i} \prod_M \prod_i^{n_M} \int d\mathbf{r}_{M_i} \int D\psi \exp(-H) \delta\left[\int d\mathbf{r} \left(\sum_P z_P \hat{\rho}_P(\mathbf{r}) f + \sum_M z_M \hat{\rho}_M(\mathbf{r})\right)\right] \quad (1)$$

where subscript  $j$  represents all species in the system and  $n_j$  is the number of molecules of species  $j$ . The contour position along the  $i$ th polymer chain of type  $P$  is designated by  $\mathbf{R}_{P_i}(s)$ , where  $s$  is a distance measured along the contour of a chain; the spatial position vector of the  $i$ th molecule of type  $M$  is  $\mathbf{r}_{M_i}$ . The microscopic density operator of species  $j$  is  $\hat{\rho}_j$ , the electrostatic potential is designated  $\psi(\mathbf{r})$ , and  $H$  is the modified Edwards Hamiltonian which can be written as  $H = H_{\text{ela}} + H_{\text{exc}} + H_{\text{ele}}$ , where

$$H_{\text{ela}} = \sum_P \sum_i^{n_P} \frac{3}{2b^2} \int_0^{N_P} ds \left( \frac{\partial \mathbf{R}_{P_i}(s)}{\partial s} \right)^2 \quad (2)$$

is the Gaussian elastic energy where  $b$  is the Kuhn length which is assumed to be the same for all chains

$$H_{\text{exc}} = \sum_P \sum_{P'} \int d\mathbf{r} \frac{1}{2} v_{PP'} \hat{\rho}_P(\mathbf{r}) \hat{\rho}_{P'}(\mathbf{r}) \quad (3)$$

is the short-ranged excluded volume interaction where  $v_{PP'}$  is the excluded volume parameter between polymer chains of type  $P$  and  $P'$  (note  $v_{PP} = (1/2 - \chi_{PS})b^3$  and  $v_{PP'} = 1/2(1 + \chi_{PP'} - \chi_{PS} - \chi_{P'S})b^3$ , where the subscript “S” denotes solvent and  $\chi_{ij}$  indicates the Flory–Huggins interaction parameter between species  $i$  and  $j$ ), and

$$H_{\text{ele}} = \beta \int d\mathbf{r} \left[ \sum_P z_P \hat{\rho}_P(\mathbf{r}) f e \psi(\mathbf{r}) + \sum_M z_M \hat{\rho}_M(\mathbf{r}) e \psi(\mathbf{r}) + \frac{\epsilon}{2} \left| \nabla \psi(\mathbf{r}) \right|^2 \right] \quad (4)$$

is the mean-field electrostatic energy of the system including all charges in the system where  $e$  is the charge of an electron, and the last term represents the electric field self-energy with  $\epsilon$  being the dielectric constant of the system (assumed constant in this work). The delta function in eq 1 enforces charge neutrality on the system. Finally, the microscopic density operators are defined as

$$\hat{\rho}_P(\mathbf{r}) = \sum_i^{n_P} \int_0^{N_P} ds \delta[\mathbf{r} - \mathbf{R}_{P_i}(s)] \quad (5)$$

$$\hat{\rho}_M(\mathbf{r}) = \sum_i^{n_M} \delta(\mathbf{r} - \mathbf{r}_{M_i}) \quad (6)$$

Inserting the identity<sup>40</sup>

$$\prod_j \left( \int D\rho_j \delta[\rho_j(\mathbf{r}) - \hat{\rho}_j(\mathbf{r})] \right) = 1 \quad (7)$$

and employing a Lagrange multiplier identity for the functional delta function<sup>40</sup> such that

$$\prod_j \left[ \int D\rho_j \int D\omega_j \exp\left(\int d\mathbf{r} \omega_j(\mathbf{r}) [\rho_j(\mathbf{r}) - \hat{\rho}_j(\mathbf{r})]\right) \right] = 1 \quad (8)$$

introduces the macroscopic density field  $\rho_j(\mathbf{r})$  which is con-

strained to the microscopic density  $\hat{\rho}_j(\mathbf{r})$  by the (purely imaginary) conjugate field  $\omega_j(\mathbf{r})$ . The following relation is substituted into eq 1 for the charge neutrality constraint

$$\delta\left[\int d\mathbf{r}\left(\sum_P z_P \hat{\rho}_P(\mathbf{r})f + \sum_M z_M \hat{\rho}_M(\mathbf{r})\right)\right] = \int d\lambda \exp(-\lambda \int d\mathbf{r}[\sum_P z_P \hat{\rho}_P(\mathbf{r})f + \sum_M z_M \hat{\rho}_M(\mathbf{r})]) \quad (9)$$

where it is then noted that  $\lambda$ , which is pure imaginary, can be absorbed into  $\psi(\mathbf{r})$  because  $\int D\psi f d\lambda g(\psi(\mathbf{r}) + \lambda) \propto \int D\psi g(\psi(\mathbf{r}))$  for any function  $g$ .<sup>40</sup> After substituting eqs 5 and 6 into eq 1, it is noticed that the polymer term in eq 4 can be rewritten as

$$\prod_P \exp\left(-\int d\mathbf{r} \beta e \psi(\mathbf{r}) z_P f \sum_i \int_0^{N_P} ds \delta[\mathbf{r} - \mathbf{R}_{P_i}(s)]\right) = \prod_P \prod_i \exp(-\beta e z_P f \int_0^{N_P} ds \psi[\mathbf{R}_{P_i}(s)]) \quad (10)$$

and the microscopic density term in eq 8 can be rewritten as

$$\prod_j \exp\left(-\int d\mathbf{r} \omega_j(\mathbf{r}) \hat{\rho}_j(\mathbf{r})\right) = \prod_P \prod_i \exp\left(-\int_0^{N_P} ds \omega_P[\mathbf{R}_{P_i}(s)]\right) \prod_M \prod_i \exp[-\omega(\mathbf{r}_{M_i})] \quad (11)$$

Finally, the partition function may be written as

$$Z = \int \prod_j (D\omega_j D\rho_j) D\psi \exp(-F) \quad (12)$$

where the dimensionless system free energy can be written, using Stirling's approximation, as

$$F = \int d\mathbf{r} \left( \frac{1}{2} \beta \epsilon \left| \nabla \psi(\mathbf{r}) \right|^2 + \sum_M \beta e \psi(\mathbf{r}) z_M \rho_M(\mathbf{r}) - \sum_j \omega_j(\mathbf{r}) \rho_j(\mathbf{r}) + \sum_P \sum_{P'} \frac{1}{2} v_{PP'} \rho_P(\mathbf{r}) \rho_{P'}(\mathbf{r}) \right) + \sum_j n_j (\ln n_j - 1) - \sum_M \sum_i \ln \left( \int D\mathbf{r}_{M_i} \exp[-\omega(\mathbf{r}_{M_i})] - \sum_P \sum_i \ln \left( \int d\mathbf{R}_{P_i} \exp \left( -\int_0^{N_P} ds \left[ \frac{3}{2b^2} \left( \frac{\partial \mathbf{R}_{P_i}(s)}{\partial s} \right)^2 + \beta e f z_P \psi(\mathbf{R}_{P_i}(s)) + \omega_P(\mathbf{R}_{P_i}(s)) \right] \right) \right) \right) \quad (13)$$

The SCF equations are obtained through use of the saddle point approximation which requires taking the functional derivatives of the free energy such that  $\delta F / \delta \psi(\mathbf{r}) = 0$ ,  $\delta F / \delta \rho_j(\mathbf{r}) = 0$ , and  $\delta F / \delta \omega_j(\mathbf{r}) = 0$ . The details of these minimizations may be found in the Appendix, but the results are

$$\omega_M(\mathbf{r}) = \beta e z_M \psi(\mathbf{r}) \quad (14)$$

$$\omega_P(\mathbf{r}) = v_P \rho_P(\mathbf{r}) + v_{PP'} \rho_{P'}(\mathbf{r}) \quad (15)$$

$$\rho_M(\mathbf{r}) = c_M \exp(-\omega_M(\mathbf{r})) \quad (16)$$

$$\rho_P(\mathbf{r}) = \frac{\sum_i^{n_P} \int ds \int d\mathbf{R}' \int d\mathbf{R}'' G_{P_i}(\mathbf{r}, \mathbf{R}', s) G_{P_i}(\mathbf{R}'', \mathbf{r}, N_P - s)}{\int d\mathbf{R}' \int d\mathbf{R}'' G_P(\mathbf{R}'', \mathbf{R}', N_P)} \quad (17)$$

$$\nabla^2 \psi(\mathbf{r}) = -\frac{1}{\epsilon} \left( \sum_P f e z_P \rho_P(\mathbf{r}) + \sum_M e z_M \rho_M(\mathbf{r}) \right) \quad (18)$$

Here,  $c_M$  is the bulk concentration of ions defined by  $c_M = n_M/V$  where electroneutrality requires (for positive polyions)  $c_- = c_+ + n_C N_C/V$ , and  $G_{P_i}(\mathbf{R}'', \mathbf{R}', N_P)$  is the Green's function defining the probability density (in units of inverse volume) of finding a segment on the  $i$ th chain of type  $P$  at a point  $\mathbf{R}''$  in space after moving  $N_P$  steps along the chain starting from the point  $\mathbf{R}'$  in space. It can be shown that the Green's function satisfies the diffusion-like equation<sup>42</sup>

$$\left( \frac{\partial}{\partial n} - \frac{b^2}{6} \nabla_{\mathbf{r}}^2 + \omega_P(\mathbf{r}) + \beta z_P f e \psi(\mathbf{r}) \right) G_{P_i}(\mathbf{r}, \mathbf{r}', n) = \delta(\mathbf{r} - \mathbf{r}') \delta(n) \quad (19)$$

where the delta functions on the right-hand side contain the initial condition.

Simplifying and adding a constant to the free energy in eq 13 gives

$$F = \int d\mathbf{r} \left( \frac{1}{2} \beta \epsilon \left| \nabla \psi(\mathbf{r}) \right|^2 - \sum_P \sum_{P'} \frac{1}{2} v_{PP'} \rho_P(\mathbf{r}) \rho_{P'}(\mathbf{r}) - \sum_M (\rho_M(\mathbf{r}) - c_M) \right) - \sum_P n_P \ln Z_P + \sum_P x_P n_T [\ln(x_P n_T) - 1] + \sum_M c_M V [\ln(c_M V) - 1] \quad (20)$$

where  $n_T$  is the total number of chains in the system defined by  $n_T = \sum_P n_P$ ,  $x_P$  is the number fraction of chains of type  $P$  defined by  $x_P = n_P/n_T$ , and  $Z_P$  is the partition function of chain type  $P$  defined by  $Z_P = \int d\mathbf{R}' \int d\mathbf{R}'' G_P(\mathbf{R}'', \mathbf{R}', N_P)$ . The integral term in eq 20 gives the self-energy of the various fields (i.e., electrostatic potential, polymer chemical potential, and small ion chemical potential relative to the bulk). The second term is the free energy associated with the chains of type  $P$ . The third term is the free energy of ideal mixing for the polymers. The final term is the free energy of ideal mixing for the small ions.

**2.2. One-Dimensional Equations.** Working in flat plate geometry, if it is assumed that the grafting density is high enough that there are not significant variations in the system properties in the directions parallel to the grafting surface, then the SCF equations can be made one-dimensional by a method similar to that of Edwards and Dolan.<sup>9</sup> For polymer brushes where the chain end is confined to the grafting surface (here defined to be the  $y$ - $z$  plane) we can define for the  $i$ th chain in the mean-field approximation

$$G_P(x, x', n) = \frac{1}{x_P \sigma} \sum_i G_{P_i}(x, y, z; x', y', z'; n) \quad (21)$$

or equivalently

$$G_P(x, x', n) = \int dy'_i \int dz'_i G_P(x, y, z; x', y'_i, z'_i; n) \quad (22)$$

where  $\sigma$  is the grafting density in number per unit area. It can be seen that only  $x'$  does not depend on  $i$  by considering the

grafting point where  $x' = 0$  for all chains. However, the location on the surface should depend on chain selected. Thus, eq 17 for the segment density of polymer type  $P$  can be rewritten as

$$\rho_P(\mathbf{r}) = x_P \sigma \frac{\int ds \int dx'' G_P(x, x', s) G_P(x'', x, N_P - s)}{\int dx'' G_P(x'', x', N_P)} \quad (23)$$

if it is assumed that the grafting point  $x'$  is at zero and remains constant. Equation 23 can be further simplified as  $\rho_P(\mathbf{r}) = x_P \sigma \rho_P(x)$ , which is normalized such that integrating the segment density over the entire volume yields the total number of segments of type  $P$  in the system given by  $N_{PN} x_P$ .

The simplified form of eq 23 can then be inserted into the diffusion equation which is integrated over  $y'_i$  and  $z'_i$  to give

$$\left( \frac{\partial}{\partial n} - \frac{b'}{2} \frac{\partial^2}{\partial x^2} + x_P \sigma \rho_P(x) v_{PP} + x_P \sigma \rho_P(x) v_{PP'} + z_P \frac{f e \psi(x)}{k_B T} \right) G_P(x, x', n) = \delta(x - x') \delta(n) \quad (24)$$

where  $b' = b/\sqrt{3}$  is the Kuhn length scaled to account for the change in dimensionality. The one-dimensional Poisson–Boltzmann equation is then

$$\frac{\partial^2 \psi}{\partial x^2} = - \frac{1}{\epsilon} \left( \sum_P z_P x_P \sigma \rho_P(x) e f + \sum_M z_M e \rho_M(x) \right) \quad (25)$$

Scaling the electric potential  $\psi$  by  $e/k_B T$  and rearranging eq 25 gives the Bjerrum length,  $l_B = e^2/\epsilon k_B T$ , as the prefactor to the left-hand side of the Poisson–Boltzmann equation. Integrating over  $y$  and  $z$  in eq 20 gives the one-dimensional system free energy,  $F$ , in units of joules per mole of chains as

$$\frac{F}{N_{\text{Av}} k_B T} = \int dx \left[ \frac{\epsilon k_B T}{2 e^2 \sigma} \left( \frac{\partial \psi(x)}{\partial x} \right)^2 - \sigma \sum_P \sum_{P'} \frac{1}{2} v_{PP'} x_P \rho_P(x) x_{P'} \rho_{P'}(x) - \sum_M (\rho_M(x) - c_M) \right] - \sum_P x_P \ln Z_P + \sum_P x_P \ln x_P \quad (26)$$

where  $N_{\text{Av}}$  is Avogadro's number. Here, the contributions to the free energy from the bulk properties of the mixed brush system which do not depend on the brush composition  $x_P$  (i.e., those contributions associated with the last two terms of eq 20) have been dropped for simplicity because these terms cancel out when calculating the free energy of mixing; see eq 27. Note the counterion concentration  $c_-$  which appears in the last term of eq 20 is in theory a function of  $x_P$  because of the ions liberated from the polyelectrolyte chains, but as the system length in the  $x$ -direction goes to infinity (as in this work), its dependence on  $x_P$  becomes negligible.

Ultimately, we are interested in the phase behavior of neutral polymer brushes mixed with polyelectrolyte brushes. Therefore, it is desirable to calculate the change in free energy due to the mixing as a function of composition for the two brush types,  $x_C$  (defined as the number fraction of the charged chains). The change in free energy,  $\Delta F_{\text{mix}}$ , is calculated in the standard way by subtracting the weighted pure component free energies from the current value:

$$\Delta F_{\text{mix}}(x_C) = F(x_C) - x_C F(x_C=1) - (1 - x_C) F(x_C=0) \quad (27)$$

**2.3. Solution Method.** The one-dimensional form of the governing equations (i.e., eqs 14–19) for the mixed polymer brushes are solved simultaneously via an iterative self-consistent method at each value of polyelectrolyte composition  $x_C$  to generate free energy of mixing curves from which the spinodal and binodal points can be determined. The two diffusion equations are evaluated at the same time by Edwards' discretization<sup>9</sup> to yield the Green's function as a function of space and chain contour. An initial guess is made by using the algorithm to solve the Gaussian case where there are no external fields and the solution does not depend on the segment density or the electric potential. A nonadsorbing surface boundary condition is applied such that  $G(x = 0, x', n) = 0$ , except for the initial condition which states that  $G(x = x', n = 0) = 1/b'$ . The Green's function is also set to zero at distances from the grafting surface longer than the contour length, and in fact we terminate the calculation at this length in order to conserve computational storage space. Once the Green's function has been determined, the segment densities are calculated using a Simpson's quadrature algorithm. The segment densities at distances longer than the chain contour length are set to zero.

The full nonlinear Poisson–Boltzmann equation can then be evaluated assuming symmetric monovalent salt and positively charged polyelectrolyte chains. This solution has traditionally been a difficulty in this type of work. We here employ a damped-inexact Newton method<sup>43</sup> which is found to converge rapidly depending upon the initial guess. The guess for the electric potential is initially a zero potential and thereafter the potential generated during the previous iteration of the self-consistency algorithm. The boundary conditions are zero surface charge which implies that the first derivative of the electric potential at the wall is zero, and at infinity the first derivative is also zero. Charge neutrality requires that the potential also reaches zero at infinity. Numerically we choose a distance  $D$  such that the dimensionless potential at this value of  $D$  is  $< 10^{-12}$ . It was found that  $D \approx 10 N b'$  worked sufficiently well. We further assumed the bulk concentrations of positive and negative small ions to be equal, since the concentration of counterions liberated from the polyelectrolyte goes to zero as  $D$  goes to infinity. Numerically the charges in the system do not sum to zero, but this is an artifact of choosing a finite distance over which to integrate the system.

Self-consistency is checked by the usual method, the new density values are checked against the previous iterations values, and if the difference is less than the specified tolerance, the new value is accepted as the solution. A damping parameter<sup>9</sup> is employed to hasten convergence. It is chosen to be less than or equal to one and defines the fraction of newly calculated density values to previous values that make up the solution returned to the beginning of the self-consistency algorithm. The value is chosen to give the fastest convergence.

The spinodal points are determined by numerically taking the second derivative of eq 27 and locating the two discrete composition values where this value switches from either positive to negative or negative to positive. The spinodal is chosen as the value of  $x_C$  halfway between these two points. The binodal points are determined by numerically taking the first derivative of eq 27 and testing the difference between all the combinations to find where the slopes are approximately equal by choosing the value halfway between two points where the difference switches sign. These sets are then checked to determine whether they possess a near common intercept and if so are designated the binodal points. This approximate approach results in a binodal curve that often appears "wavy".

Obviously, a smaller step size yields more precise values for the spinodal and binodal points. In regions where the two-phase region is large,  $\sim 100$  steps in  $x_C$  would suffice. Near the critical point, however, 400–500 points were often necessary.

The critical points, presented later in Figure 7 (plotted as a function of grafting density and charge fraction for various salt concentrations), were found using a bounded golden search algorithm to minimize the difference between the compositional locations of the spinodal points at a given charge fraction; points outside the two phase window were assigned a difference of one.<sup>44</sup> The grafting density was adjusted between the bounds minimizing the spinodal point difference until the change in grafting density was less than the specified tolerance, typically  $10^{-8}$ . The average was then taken and assigned as the critical point.

### 3. Results and Discussion

#### 3.1. Conformational Properties of the Mixed Brushes:

**Literature Comparisons.** The validity of the SCF model and the solution algorithm described in the previous section was first evaluated by comparing the estimated segment density profiles for pure polyelectrolyte brushes with the published results of a previous model of von Goeler and Muthukumar.<sup>22</sup> In this previous model, the electrostatic potential between charged monomers is approximated using the Debye–Hückel theory (i.e., the solution of the linearized Poisson–Boltzmann equation in spherical coordinates) with an assumption of the bulklike counterion screening of the Coulomb potential within the brush layer. Figure 2a summarizes the predictions of our model for the one-dimensional segment density, defined as  $\rho(x) = \rho(\mathbf{r})b^3/\sigma$ , of a pure polyelectrolyte brush of length  $N = 33$  in  $\Theta$  solvent with a charge fraction of unity and grafting density of  $\sigma = 0.00893 \text{ \AA}^{-2}$ . These parameter values were chosen to make the conditions as similar as possible to those used in the previous study of von Goeler and Muthukumar for a direct comparison of the results. Presented in Figure 2a are the resultant brush density profiles predicted for four different values of the average inverse screening length in the bulk limit (i.e.,  $\kappa = 4, 2, 1, 0.5$ ) defined by

$$\kappa = \left( \frac{e^2}{\epsilon k_B T} \sum_M z_M^2 C_M \right)^{1/2} \quad (28)$$

where  $e$  is the unit electron charge,  $z_M$  is the ion valence,  $C_M$  is the bulk concentration of small ions of type  $M$  in solution, and here the temperature is chosen to be  $T = 25 \text{ }^\circ\text{C}$ ; in all other modeling it is chosen to be  $T = 37 \text{ }^\circ\text{C}$ . As shown in the figure, the results show the expected behavior of a general flattening and broadening of the profile as the screening length increases, causing an increase in the electrostatic forces which results in chain swelling due to repulsion of the like charges on the chain. On the quantitative level, our results are also in reasonable agreement with the previous results obtained on the basis of the “bulklike” Debye–Hückel approximation which are also included in Figure 2b. For large values of  $\kappa$  (i.e.,  $\kappa = 4$  and 2 in units of  $1/b$ ), our model predicts a lower degree of polyelectrolyte stretching, because we solve the full non-linear Poisson–Boltzmann equation without any assumption regarding the counter-ion distribution in our model. Also, our model takes into account both the entropy of the small ions (see the second path integral in eq 1 for the canonical partition function, i.e.,  $\prod_{M,i} \int d\mathbf{r}_{Mi}$ ) and their contributions to the electrostatic energy of the system (eq 4), and this leads to a prediction of more

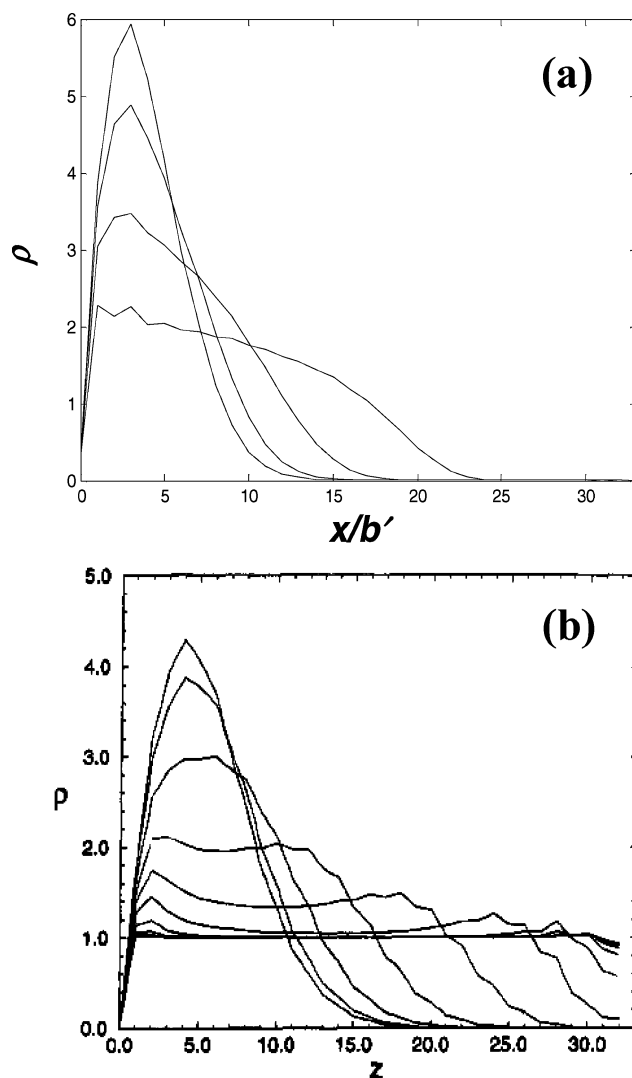


**Figure 2.** (a) Segment density,  $\rho$ , profiles of pure, completely charged polyelectrolyte brushes of length  $N = 33$  for increasing average screening length at grafting density  $\sigma = 0.00893 \text{ \AA}^{-2}$ . Here  $\rho$  is used in units of number per length of the segment (i.e.,  $1/b$ ). Setting the Kuhn length,  $b$ , to unity matches von Goeler and Muthukumar's dimensionless Coulombic interaction parameter  $\nu = 0.03125$ .<sup>22</sup> (b) Results of von Goeler and Muthukumar for  $\nu = 0.03125$  (reproduced from ref 22). In both plots (a) and (b), the least stretched distribution corresponds to an inverse Debye length of  $\kappa = 4/b$ , and each subsequent curve represents a 2-fold decrease in  $\kappa$ .

stretched conformations at lower  $\kappa$  (e.g.,  $\kappa = 0.5$ ), i.e., for the so-called osmotic brush regime in which the localization of the counterions near the brush causes additional stretching of the chains due to the corresponding osmotic pressure buildup within the brush layer.<sup>13,17</sup>

For brushes composed of two types of chains that are mutually immiscible, our model predicts nanoscopic phase separations perpendicular to the grafting surface such as have been previously reported.<sup>27,29–31</sup> In a randomly mixed brush of two incompatible polymers that are end-grafted at fixed positions on the surface, the covalent anchoring of the chains prevents macroscopic phase separation, and instead the segregation between incompatible brushes leads to the formation of lateral compositional heterogeneities at molecular length scales; morphologies that can occur in such systems include regularly arrayed globules (“dimples”) and cylinders (“ripples”) of alternating composition.<sup>27,29–31</sup> In the present study, we do not intend to investigate the lateral structuring of the nanophase-separated brushes, but rather we assume that each type of chain

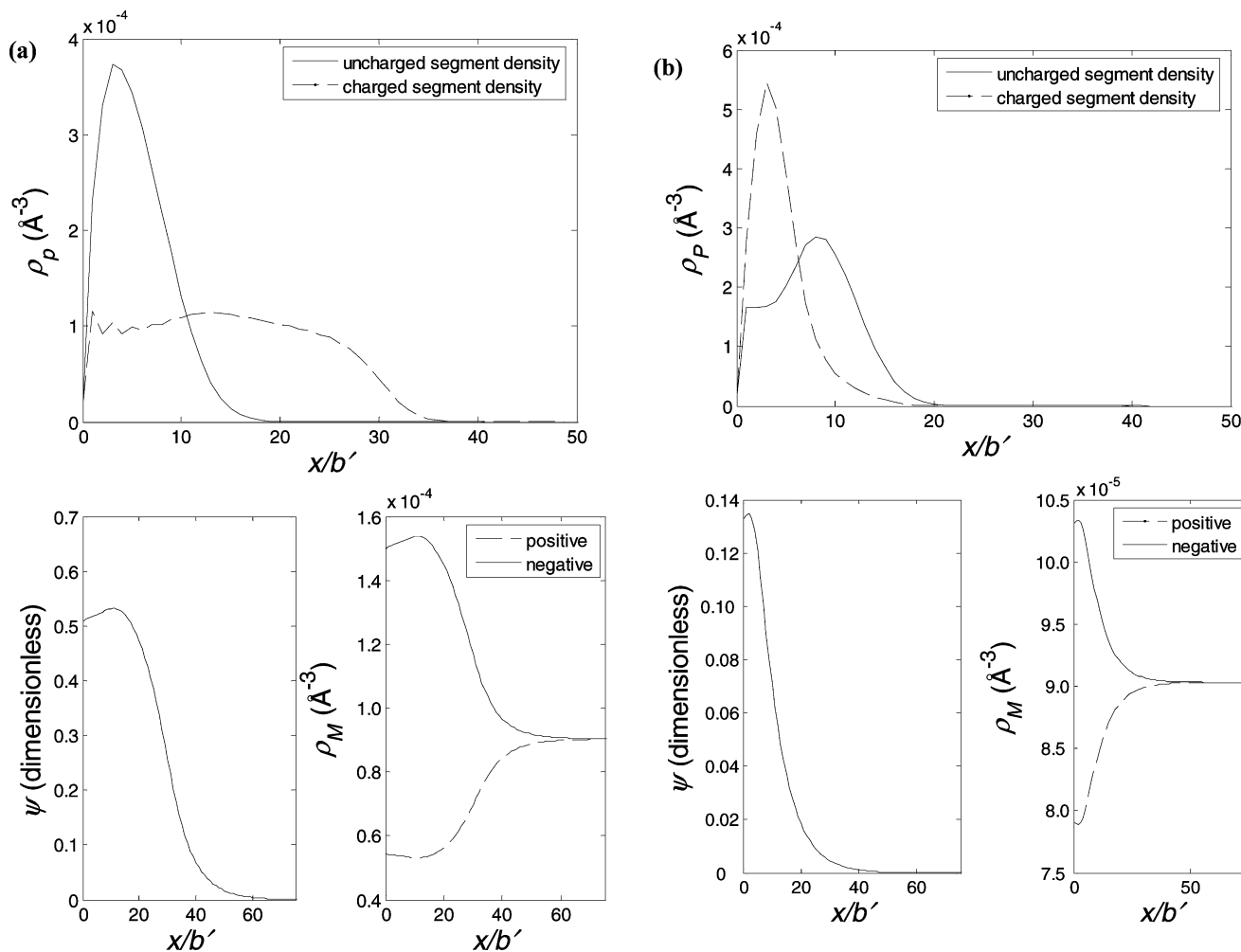


**Figure 3.** Segment density profiles illustrating change in vertical separation for chain length  $N = 49$ , Kuhn length  $b = 7 \text{ \AA}$ , grafting density  $\sigma = 0.0005 \text{ \AA}^{-2}$ , excluded volume interactions  $v_{AA} = 125 \text{ \AA}^3$ ,  $v_{AC} = 200 \text{ \AA}^3$ ,  $v_{CC} = 10 \text{ \AA}^3$ , and charge fractions on the polyelectrolyte chains (a)  $f = 1$ , (b)  $f = 0.01$ . Also included are the electrostatic potential  $\psi$  and small ion density  $\rho_M$  profiles where the bulk salt concentration is  $c_M = 150 \text{ mM}$ .

experiences an average (“mean-field”) potential that is laterally uniform and allowed to vary only along the vertical direction, which still allows us to probe vertical segregation between the dissimilar polymers. Recently, it has been reported that a pH-responsive ampholyte surface can be created by coating the surface with a mixed polyelectrolyte brush, consisting of cationic and anionic chains, which exhibits switching of the segregated brush compositions in the direction normal to the grafting surface with changes in pH.<sup>45</sup> For mixed brushes between charged and neutral polymers, our modeling suggests a similar possibility of separation of segment populations along the vertical axis between the two components under certain interaction conditions. Figure 3a,b illustrates the perpendicular phase separation for mixed charged and neutral chains of identical length  $N = 49$  and at an overall grafting density of  $\sigma = 0.0005 \text{ \AA}^{-2}$ . The two chain types illustrated in these figures are assumed to have a strong polymer–polymer cross-interaction exemplified by the excluded volume parameter  $v_{AC} = 200 \text{ \AA}^3$  (which is comparable to the monomer volume  $b^3 \gg 343 \text{ \AA}^3$ ) so that the tendency for the fixed end-grafted polymers would be to phase segregate on the molecular level. Also, the like-molecule interaction parameters used are  $v_{AA} = 125 \text{ \AA}^3$  and  $v_{CC} = 10 \text{ \AA}^3$  for the neutral and charged chains, respectively. As shown in Figure 3b, when the charge fraction on the polyelectrolyte chains is small (i.e.,  $f = 0.1$ ), the neutral chains are more swollen because they have the larger excluded volume parameter. However, when the charge fraction is increased (as demonstrated

in Figure 3a for the case of  $f = 1$ ), the polyelectrolyte chains swell and force the neutral chains to collapse. This observed trend in the vertical phase separation can be summarized in terms of the relative strength of the two external field interactions; the more stretched chain type is the one having the stronger combined field interactions. Our results also suggest that one can design a surface that is switchable in its chemistry at the outermost surface between charged and neutral states using the perpendicular phase separation mechanism achievable using ionic/neutral mixed brushes (in response to a change in the charge fraction on the polyelectrolyte chains which could be controlled by a change in pH); a detailed discussion of the quantitative design criteria for this reversible (vertical) conformational switching in mixed brushes containing charged and noncharged polymers is a subject of our future publication.

Also included in Figure 3a,b are plots of the electrostatic potential and small ion distributions. The potential shows the correct limiting behavior by decaying to zero at large distances because of the (average) charge neutrality in the bulk. The ion distributions show a cloud enriched in counterions and depleted in co-ions in the region containing the end-grafted polymers. Both distributions asymptotically approach the bulk limit at large distances.

**3.2. Macroscopic Phase Behavior of the Mixed Brushes: Effect of Charge.** If we now allow the grafting points to move along the surface, the macroscopic phase separation can be realized in a neutral and polyelectrolyte brush mixture. Using

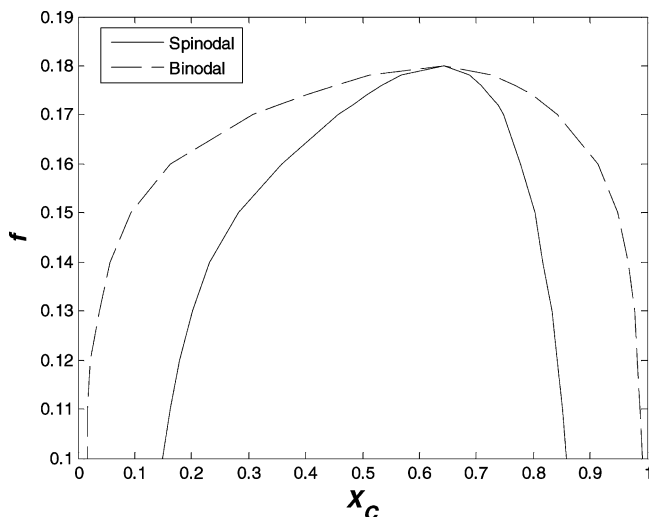


**Figure 4.** Phase diagram illustrating increased miscibility with increasing polyelectrolyte charge fraction  $f$  as a function of composition  $x_c$  for chains of length  $N = 49$  with Kuhn length  $b = 7 \text{ \AA}$ , grafting density  $\sigma = 0.0005 \text{ \AA}^{-2}$ , excluded volume interactions  $v_{AA} = 125 \text{ \AA}^3$ ,  $v_{AC} = 215 \text{ \AA}^3$ ,  $v_{CC} = 100 \text{ \AA}^3$ , and bulk salt concentration  $c_M = 150 \text{ mM}$ .

the formalism for the free energy change of mixing (eq 27), we performed an analysis on the composition-dependent thermodynamic stability of the single-phase (mixed) states in the mixed brushes under various charge and grafting conditions. In this section, we will discuss the influence of variation in the effective electrostatic potential (acting on the polyelectrolyte chains) on the two-dimensional macroscopic phase behavior of the system. For demonstration of the general patterns of behavior, we consider a binary mixture of charged and neutral brushes with chain lengths  $N = 49$ , end-grafted to a surface at an overall grafting density of  $\sigma = 0.0005 \text{ \AA}^{-2}$ . The excluded volume parameters for these polymers were chosen as  $v_{AA} = 125 \text{ \AA}^3$ ,  $v_{CC} = 100 \text{ \AA}^3$ , and  $v_{AC} = 215 \text{ \AA}^3$  (with the subscript “A” and “C” denoting the neutral and charged species, respectively) such that interesting phase behavior can be found as the charge fraction ( $f$ ) is varied between 0 and 1; these values of the excluded volume indicate that the solvent is good for both chain types, and there exists a strong repulsion between the different segment types. Under the given parameter values, the key factor that determines mixing of the brushes is the effective amount of charge in the system which depends on the charge fraction of the polyelectrolyte chains and on the amount of salt added to the system ( $C_M$ ). To elucidate the effect of the charge content of the polyelectrolyte chain on the macrophase separation, we first fix the concentration of added salt in the bulk at  $C_M = 150 \text{ mM}$  and the temperature to be  $T = 37 \text{ }^\circ\text{C}$  (which are close to the physiological conditions). The Bjerrum length for water is  $l_B = 6.7 \text{ \AA}$  at these conditions. Figure 4 presents a plot of composition spinodal and binodal points for various values of the charge fraction. We here see an upper critical charge fraction,  $f_c \gg 0.18$ , with a region of instability enveloped by a metastable region which opens downward as  $f$  is decreased. Thus, we see that by increasing the fractional charge per polyelectrolyte segment the miscibility increases rapidly. This effect is due to the fact that increasing the charge on the chains increases the energy penalty of having like charges in close proximity if the chains are phase separated. However, if the chains are mixed, the neutral segments are able to get in between the charged segments and increase the distance separating the charges, thus lowering the energy penalty.

The macroscopic phase separation of the mixed brush system cannot necessarily be inferred from the segment density distributions calculated for the corresponding parameters (assuming fixed grafting end points). We checked the brush density profiles inside and outside of the two phase region on the  $f$ - $x_c$  phase diagram (Figure 4) and also on other phase diagrams shown in Figures 5 and 6 which will be discussed later in this paper. In all cases, there were in general only very subtle differences in the density profiles. See Figure S1 in the Supporting Information for representative segment density profiles both outside and inside the two-phase envelope shown in Figure 4.

The location of the critical charge fraction ( $f_{\text{crit}}$ ) was found to be sensitively dependent upon the values of the excluded volume parameters, especially the one that characterizes the polymer cross-interaction. For instance, as the excluded volume repulsion between the two components increases at fixed solvent quality for individual brushes the critical charge fraction also increases. In the case of a solvent where there are no excluded volume cross-interactions (assuming that the effects of three-body interactions are negligible), the critical point vanishes, and the brushes become miscible in all proportions at all values of  $f$ . In general, increasing the cross-interactions decreases miscibility due to heightened repulsion between the polymer types, while increasing the individual excluded volume interactions increases miscibility due to the reduced net attraction between the like molecules. Representative phase diagrams which illustrate these points are presented in Figures S2–S4 in the Supporting Information. The two-dimensional phase behavior is controlled largely by a balancing between the excluded volume repulsion between the two brush types (which favors demixing) and dilution of the polyelectrolyte charges (which favors mixing).

The phase separation in the mixed brush yields two macroscopically separated domains with one being rich in the polyelectrolyte component and the other depleted in the polyelectrolyte. The phase diagram shown in Figure 4 is slightly asymmetric with the critical composition lying in the polyelectrolyte-rich region. It can be shown a posteriori that this asymmetry is primarily due to the higher external potential that acts on the polyelectrolyte brush in its unmixed state than that for the neutral brush in the corresponding state. Because of this inequality of the pure-state external potential, the polyelectrolyte has a greater tendency to be incorporated into the neutral-rich phase than the neutral chain has toward the polyelectrolyte-rich phase, and therefore the phase diagram becomes asymmetric toward polyelectrolyte-rich compositions. A quantitative discussion can be made in terms of the average chain interaction (in units of  $k_B T$ ) that a brush segment of type  $P$  would have with its external fields defined by

$$\langle \bar{U}_{\text{ext}} \rangle_P = \frac{1}{V} \int d\mathbf{r} [\omega_P(\mathbf{r}) + \beta z_{Pf} e \psi(\mathbf{r})] \quad (29)$$

Using the physical picture described above, we examined the difference  $\langle \bar{U}_{\text{ext}} \rangle_{P,x_p=0} - \langle \bar{U}_{\text{ext}} \rangle_{P,x_p=1}$  which (to a reasonable approximation) measures the change of the average interaction potential per segment upon transferring a brush chain of type  $P$  from its pure state to a state in which the chain is surrounded by the other type of polymers. Note that this value is normally positive under phase-separated conditions. Calculating this difference for various combinations of excluded volume and electrostatic interactions and comparing to a corresponding free energy of mixing plot (results not shown), we confirmed that the pure component with the smaller difference (i.e., the component that has a larger value for  $\langle \bar{U}_{\text{ext}} \rangle_{P,x_p=1}$ , given that

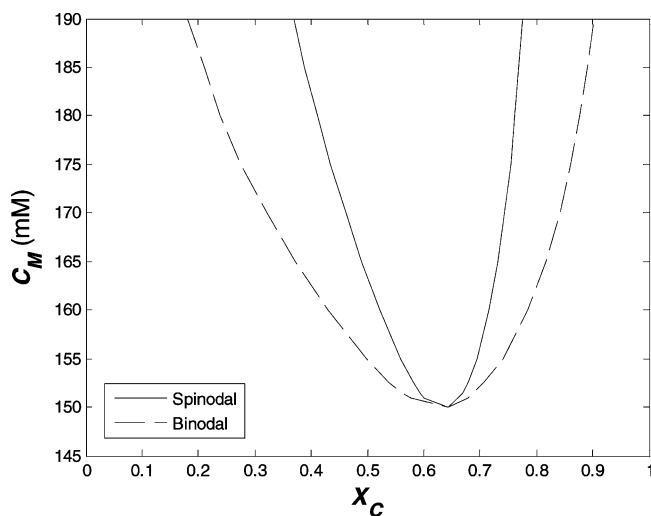


**Figure 5.** Phase diagram showing decreased miscibility with increasing bulk salt concentration  $c_M$  as a function of composition  $x_c$  for chains of length  $N = 49$  with Kuhn length  $b = 7 \text{ \AA}$ , grafting density  $\sigma = 0.0005 \text{ \AA}^{-2}$ , excluded volume interaction  $v_{AA} = 125 \text{ \AA}^3$ ,  $v_{AC} = 215 \text{ \AA}^3$ ,  $v_{CC} = 100 \text{ \AA}^3$ , and polyelectrolyte charge fraction  $f = 0.18$ .

$\langle \bar{U}_{\text{ext}} \rangle_{P, x_P=0} \approx \langle \bar{U}_{\text{ext}} \rangle_{P', x_{P'}=0}$ ) is the species toward which the two-phase envelope becomes shifted. Thus, if the neutral chain excluded volume was large enough compared to the combined excluded volume and electrostatic effects of the polyelectrolyte, the phase diagram would be asymmetric toward the neutral chain. See Figure S5 in the Supporting Information for an example.

The other important parameter which controls the net impact of the polyelectrolyte charge and thus the miscibility of the two brush types is the amount of small salt ions added to the solution. Increasing the amount of salt in the solution will decrease the effective amount of charge each segment feels from surrounding charges due to screening effects, and thus we expect that adding salt would be akin to reducing the charge fraction per segment which has been shown to reduce the miscibility of the two chain types in the brush. Figure 5 is a phase diagram for added salt concentration,  $C_M$ , as a function of composition. For this calculation, we used an overall grafting density of  $\sigma = 0.0005 \text{ \AA}^{-2}$  with a polyelectrolyte charge fraction of  $f = 0.18$ , and the remaining parameters (i.e.,  $N$ ,  $v_{AA}$ ,  $v_{CC}$ , and  $v_{AC}$ ) were chosen to be the same as in the previous example in Figure 4. As expected, the two-phase region opens upward from a lower critical salt concentration ( $C_{M,c}$ ), as the average screening length is reduced. For the given set of conditions, this critical value is found to be around  $C_{M,c} \gg 150 \text{ mM}$ , which corresponds to the same critical point found above.

**3.3. Macroscopic Phase Behavior of the Mixed Brushes: Effect of Grafting Density.** In a mixed brush system where the two polymers are highly repulsive, the effect of grafting density on the miscibility of the brushes is to favor demixing as the number of chains per unit area increases. This result is anticipated because the chains have a strong repulsion for each other due to the excluded volume cross-interaction term whose effects will increase as the number of segments in the same volume increases. Obviously, increasing the strength of this interaction will increase this effect. Figure 6 presents a representative phase diagram for the overall grafting density,  $\sigma$ , vs composition,  $x_c$  (i.e., the number fraction of the charged chains), with polyelectrolyte charge fraction  $f = 0.18$ . Again, the values used for  $N$ ,  $v_{AA}$ ,  $v_{CC}$ , and  $v_{AC}$  are the same as in the previous cases for Figures 4 and 5, and the temperature of  $T = 37 \text{ }^\circ\text{C}$  and the added salt concentration of  $C_M = 150 \text{ mM}$  are

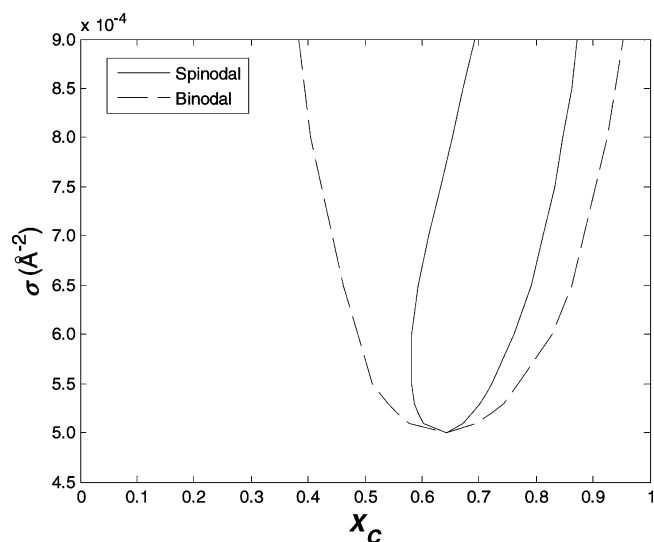


**Figure 6.** Phase diagram demonstrating decreased miscibility with increased grafting density  $\sigma$  as a function of composition  $x_c$  for chains of length  $N = 49$  with Kuhn length  $b = 7 \text{ \AA}$ , charge fraction on the polyelectrolyte chains  $f = 0.18$ , excluded volume interactions  $v_{AA} = 125 \text{ \AA}^3$ ,  $v_{AC} = 215 \text{ \AA}^3$ ,  $v_{CC} = 100 \text{ \AA}^3$ , and bulk salt concentration  $c_M = 150 \text{ mM}$ .

used in Figure 6. As shown in the figure, there exists a lower critical density,  $\sigma_c \approx 5.0 \times 10^{-4} \text{ \AA}^{-2}$ , below which the two brush types are miscible in all proportions, but above this point separation begins to occur. The region of instability that opens from the critical point as the grafting density increases has a unique shape. It is seen to lean toward the polyelectrolyte-rich region of the plot, and the miscibility gap appears to reduce back mildly with increasing grafting density above a certain level. It is not feasible to determine whether these trends continue at higher grafting densities (above what is displayed in the figure) because the SCF approximations break down at high grafting densities where the interactions with the external fields become much larger than  $k_B T$ . Our modeling indicates that the anomalous shape of the spinodal curve persists over a range of parameter values, for example, for  $f$  and  $C_M$ , and at present we do not have any clear explanation for this behavior. Nonetheless, the results clearly demonstrate the effect that the grafting density has on the two-dimensional phase behavior of the mixed brushes; as the grafting density is increased, the short-range repulsion (which favors phase separation) comes to dominate the forces that favor mixing at low values of  $\sigma$  (such as the screened Coulombic repulsion between the charged segments on the polyelectrolyte chains), and as a consequence, phase separation occurs in the system.

**3.4. Macroscopic Phase Behavior of the Mixed Brushes: Combined Effects.** Plotting the critical values of the grafting density against their corresponding critical charge fractions provides a useful tool for understanding and summarizing the above mixed polymer brush phase separation trends. Figure 7 shows how the critical grafting density,  $\sigma_{\text{crit}}$ , changes as a function of the critical charge fraction,  $f_{\text{crit}}$ , for various values of the bulk salt concentration,  $c_M$ . The values of  $N$ ,  $v_{AA}$ ,  $v_{AC}$ , and  $v_{CC}$  were the same as in the previous subsections; the salt concentrations used were 150 mM for the upper most curve and 200, 250, 500, and 1000 mM respectively for each subsequently lower curve. For all salt concentrations, a higher critical charge fraction corresponds to a larger critical grafting density; in fact, the increase is greater than exponential. This agrees with the above finding that increased charging favors mixing of the brushes due to the dilution effect of the polyelec-

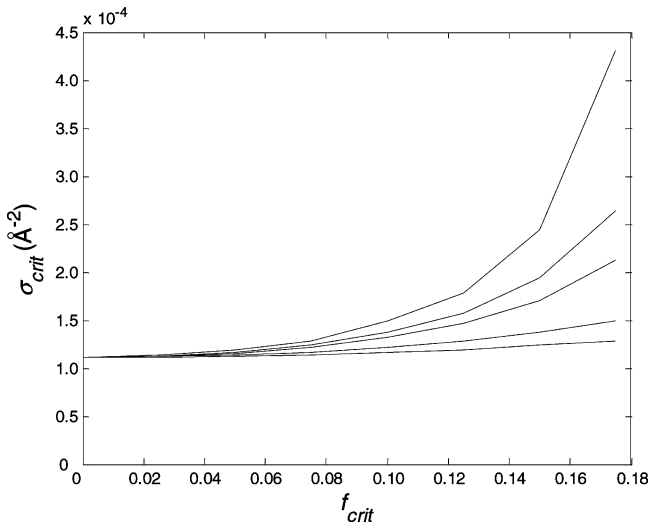


**Figure 7.** Plot of critical grafting density,  $\sigma_{\text{crit}}$ , vs critical charge fraction,  $f_{\text{crit}}$ , at various bulk salt concentrations,  $c_M$ , showing how grafting density must be increased to induce separation at larger charge fractions. Beginning with the upper most curve the salt concentrations are  $c_M = 150, 200, 250, 500,$  and  $1000$  mM with chains of length  $N = 49$  and Kuhn length  $b = 7 \text{ \AA}$ , excluded volume interactions  $v_{AA} = 125 \text{ \AA}^3$ ,  $v_{AC} = 215 \text{ \AA}^3$ ,  $v_{CC} = 100 \text{ \AA}^3$ .

trolyte brushes in the neutral brushes. Also, as expected, increasing the bulk salt concentration at fixed critical charge fraction lowers the critical grafting density due to the screening effect of the small ions. All curves have the same y-intercept (because, in the neutral limit, the added small ions have no influence on the phase behavior of the mixed brushes), and a plot at infinite bulk salt concentration (i.e., in the limit of complete screening of the electrostatic interactions) would be a horizontal line.

#### 4. Summary and Conclusions

In this work, we have developed an SCF theory for the examination of polymer brushes composed of a mixture of polyelectrolyte and neutral chains. We present a derivation of the general free energy formalism expressed in terms of the polyelectrolyte Green's function (from the canonical partition function of the system) and also an algorithm for numerically solving the set of coupled self-consistent equations (which include the diffusion equation for the Green's function and the Poisson–Boltzmann equation for the electric potential in its full nonlinear form). Within the assumption of lateral mean field, the model predicts vertical conformational segregation in the mixed brushes under the presence of strong excluded volume cross-interactions. Considering the chains to have mobile grafting points along the surface allowed for the calculation of the free energy of mixing for the two chain types. Using this result, the limits of stability could be determined for macroscopic phase separation. The phase behavior of these mixed polymer brushes in good solvent is explored as a function of smeared charge fraction ( $f$ ), added salt concentration ( $C$ ), and grafting density ( $\sigma$ ).

The presence of charge on the polyelectrolyte chains is found to strongly increase the miscibility of the two brush types that are mutually repulsive in agreement with the published results of Khokhlov and Nyrkova.<sup>41</sup> Increasing the amount of effective charge felt by each charged segment by either increasing the charge fraction per segment or increasing the screening length by removing salt ions will favor mixing of the brushes. This preference for a mixed state derives from the effective dilution of the charged chains by the neutral polymers. Increasing the grafting density is shown to decrease the miscibility of the two

chain types. Demixing is favored because decreasing the area per chain brings the chains closer together which increases the energy penalty associated with the excluded volume parameter, and a strong polymer cross-interaction will force phase separation.

#### Appendix

The derivation of the SCF equations (i.e., eqs 14–18) is accomplished by taking the functional derivative, in the saddle point approximation, of the system free energy defined by eq 13 with respect to the small ion and polymer densities and chemical potentials as well as the electrostatic potential. The functional saddle point is found through application of the Euler equations from the calculus of variations<sup>46</sup>

$$\frac{\partial f}{\partial y_i} - \frac{d}{dx} \frac{\partial f}{\partial y_{ix}} = 0 \quad i = 1, 2, \dots, n \quad (\text{A.1})$$

where  $f$  is a function of  $y_1(x), y_2(x), \dots, y_n(x)$  and  $x$ , and  $y_{ix}$  denotes  $\partial y_i(x)/\partial x$ . In this development, the subscripts  $M$  or  $P$  refer to only one type at a time (i.e.,  $M$  refers to either positive or negative small ions) since the development is identical for all  $M$  or  $P$ .

The chemical potentials can be found by directly applying eq A.1 to eq 13 where  $y_i = \rho_j$ :

$$\frac{\partial F}{\partial \rho_M} = 0 \Rightarrow -\omega_M(\mathbf{r}) + \beta e \psi(\mathbf{r}) z_M = 0 \quad (\text{A.2})$$

$$\omega_M(\mathbf{r}) = \beta e \psi(\mathbf{r}) z_M \quad (\text{A.3})$$

$$\frac{\partial F}{\partial \rho_P} = 0 \Rightarrow -\omega_P(\mathbf{r}) + v_{PP} \rho_P(\mathbf{r}) + v_{PP'} \rho_{P'}(\mathbf{r}) = 0 \quad (\text{A.4})$$

$$\omega_P(\mathbf{r}) = v_{PP} \rho_P(\mathbf{r}) + v_{PP'} \rho_{P'}(\mathbf{r}) \quad (\text{A.5})$$

The species densities can be found by applying eq A.1 to eq 13 where  $y_i = \omega_j$ :

$$\frac{\partial F}{\partial \omega_M(\mathbf{r})} = \frac{\partial}{\partial \omega_M(\mathbf{r})} \left[ - \int d\mathbf{r} \omega_M(\mathbf{r}) \rho_M(\mathbf{r}) - \sum_i^{n_M} \ln \left( \int D\mathbf{r}_{Mi} \exp[-\omega_M(\mathbf{r}_{Mi})] \right) \right] = 0 \quad (\text{A.6})$$

Assuming the  $n$  particles of type  $M$  are indistinguishable, we can write

$$\frac{\partial}{\partial \omega_M(\mathbf{r})} \left[ \ln \left( \exp \left[ - \int d\mathbf{r} \omega_M(\mathbf{r}) \rho_M(\mathbf{r}) \right] \right) - \ln \left( \int D\mathbf{r}_M \exp[-\omega_M(\mathbf{r}_M)]^{n_M} \right) \right] = 0 \quad (\text{A.7})$$

Assuming that the small ions are volumeless, we can write

$$\int D\mathbf{r}_M \exp[-\omega_M(\mathbf{r}_M)] \approx \frac{1}{V} \int d\mathbf{r} \exp[-\omega_M(\mathbf{r})] \quad (\text{A.8})$$

Then

$$\frac{\partial}{\partial \omega_M(\mathbf{r})} \left[ \ln \left( \exp \left[ - \int d\mathbf{r} \omega_M(\mathbf{r}) \rho_M(\mathbf{r}) \right] \right) - \ln \left( \left( \frac{1}{V} \int d\mathbf{r} \exp[-\omega_M(\mathbf{r})] \right)^{n_M} \right) \right] = 0 \quad (\text{A.9})$$

Introducing the bulk ion concentrations  $c_M$  and letting  $V \rightarrow \infty$ ,

we have for the second term in eq A.9

$$\left(\frac{1}{V} \int d\mathbf{r} \exp[-\omega_M(\mathbf{r})]\right)^{NM} = \left(1 + \frac{1}{V} \int d\mathbf{r} (\exp[-\omega_M(\mathbf{r})] - 1)\right)^{NM} \approx (\exp[\int d\mathbf{r} (\exp[-\omega_M(\mathbf{r})] - 1)])^{NM} \quad (\text{A.10})$$

which is due to  $\lim_{n \rightarrow \infty} (1 + x/n)^n = e^x$ . Thus

$$\frac{\partial}{\partial \omega_M(\mathbf{r})} \left[ \int d\mathbf{r} (-\omega_M(\mathbf{r}) \rho_M(\mathbf{r}) - c_M \exp[-\omega_M(\mathbf{r})] + c_M) \right] = 0 \quad (\text{A.11})$$

Finally

$$\rho_M(\mathbf{r}) = c_M \exp[-\omega_M(\mathbf{r})] \quad (\text{A.12})$$

Similarly, the polymer segment densities can be found from

$$\frac{\partial F}{\partial \omega_p(\mathbf{r})} = \frac{\partial}{\partial \omega_p(\mathbf{r})} \left\{ \int d\mathbf{r} (-\omega_p(\mathbf{r}) \rho_p(\mathbf{r})) - \sum_i^{n_p} \ln \left[ \int d\mathbf{R}_{p_i} \exp\left(-\int_0^{N_p} ds \Omega_p[\mathbf{R}_{p_i}(s)]\right) \right] \right\} = 0 \quad (\text{A.13})$$

where

$$\Omega_p[\mathbf{R}_{p_i}(s)] = \frac{3}{2b^2} \left( \frac{\partial \mathbf{R}_{p_i}}{\partial s} \right)^2 + \beta e f z_p \psi[\mathbf{R}_{p_i}(s)] + \omega_p[\mathbf{R}_{p_i}(s)] \quad (\text{A.14})$$

Again assuming the chains are indistinguishable

$$\frac{\partial}{\partial \omega_p(\mathbf{r})} \left\{ \int d\mathbf{r} [-\omega_p(\mathbf{r}) \rho_p(\mathbf{r})] - \ln \left[ \int d\mathbf{R}_p \exp\left(-\int_0^{N_p} ds \Omega_p[\mathbf{R}_p(s)]\right) \right]^{n_p} \right\} = 0 \quad (\text{A.15})$$

We now let

$$\int d\mathbf{R}_p \exp\left(-\int_0^{N_p} ds \Omega_p[\mathbf{R}_p(s)]\right) = \int d\mathbf{R}' \int d\mathbf{R}'' \int_{\mathbf{R}_p(0)=\mathbf{R}'}^{\mathbf{R}_p(N_p)=\mathbf{R}''} \delta \mathbf{R}_p \exp\left(-\int_0^{N_p} ds \Omega_p[\mathbf{R}_p(s)]\right) \quad (\text{A.16})$$

The Green's function can now be defined and substituted into eq A.16 to give for the right-hand side

$$\int d\mathbf{R}' \int d\mathbf{R}'' \frac{K}{V} G_p(\mathbf{R}'', \mathbf{R}', N_p) \quad (\text{A.17})$$

where  $K$  is an arbitrary constant that ensures dimensionality and normalization. Utilizing properties of integration and the Green's function,<sup>42</sup> we can write for expression A.17

$$\frac{1}{N_p} \int_0^{N_p} ds \int d\mathbf{R}' \int d\mathbf{R}'' \frac{K}{V} \int d\mathbf{r} G_p(\mathbf{r}, \mathbf{R}', s) G_p(\mathbf{R}'', \mathbf{r}, N_p - s) \quad (\text{A.18})$$

Defining  $\Gamma_p(\mathbf{r})$  for simplicity (A.18) reduces to

$$\frac{K}{V} \int d\mathbf{r} \Gamma_p(\mathbf{r}) \quad (\text{A.19})$$

Inserting (A.19) into (A.15) yields

$$\frac{\partial}{\partial \omega_p(\mathbf{r})} \left\{ \int d\mathbf{r} [-\omega_p(\mathbf{r}) \rho_p(\mathbf{r})] - \ln \left[ \left(1 + \frac{K}{V} \int d\mathbf{r} \left(\Gamma_p(\mathbf{r}) - \frac{1}{K}\right)^{V c_p}\right) \right] \right\} = 0 \quad (\text{A.20})$$

where the bulk polymer concentration is defined as  $c_p = n_p/V$ . This can be approximated for  $V \rightarrow \infty$  as

$$\frac{\partial}{\partial \omega_p(\mathbf{r})} \left\{ \int d\mathbf{r} \left(-\omega_p(\mathbf{r}) \rho_p(\mathbf{r}) - c_p K \left[\Gamma_p(\mathbf{r}) - \frac{1}{K}\right]\right) - \rho_p(\mathbf{r}) - \frac{n_p}{V} K \frac{\partial \Gamma_p(\mathbf{r})}{\partial \omega_p(\mathbf{r})} \right\} = 0 \quad (\text{A.21})$$

because  $\exp(x) \approx (1 + \{x\}/\{n\})^n$  for large  $n$ . The derivative in the center of (A.21) can be evaluated as

$$\frac{\partial \Gamma_p(\mathbf{r})}{\partial \omega_p(\mathbf{r})} = \frac{1}{N_p} \int ds \int d\mathbf{R}' \int d\mathbf{R}'' \frac{\partial}{\partial \omega_p(\mathbf{r})} [G_p(\mathbf{r}, \mathbf{R}', s) G_p(\mathbf{R}'', \mathbf{r}, N_p - s)] \quad (\text{A.22})$$

where

$$\frac{\partial}{\partial \omega_p(\mathbf{r})} G_p(\mathbf{r}, \mathbf{R}', s) = \int_{\mathbf{R}_p(0)=\mathbf{R}'}^{\mathbf{R}_p(s)=\mathbf{r}} \delta \mathbf{R}_p(s) \exp\left(-\int_0^s ds' \Omega_p[\mathbf{R}_p(s')]\right) \left(-\int_0^s ds' \frac{\partial \Omega_p[\mathbf{R}_p(s')]}{\partial \omega_p(\mathbf{r})}\right) = G_p(\mathbf{r}, \mathbf{R}', s)(-s) \quad (\text{A.23})$$

because  $\partial \Omega_p[\mathbf{R}_p(s)]/\partial \omega_p(\mathbf{r}) = 1$  when  $\mathbf{R}_p(s) = \mathbf{r}$  for any  $s$  along the chain as required by the functional contour integral, and similarly

$$\frac{\partial}{\partial \omega_p(\mathbf{r})} G_p(\mathbf{R}'', \mathbf{r}, N_p - s) = G_p(\mathbf{R}'', \mathbf{r}, N_p - s)[- (N_p - s)] \quad (\text{A.24})$$

Thus

$$\rho_p(\mathbf{r}) = n_p \frac{K}{V} \int ds \int d\mathbf{R}' \int d\mathbf{R}'' G_p(\mathbf{r}, \mathbf{R}', s) G_p(\mathbf{R}'', \mathbf{r}, N_p - s) \quad (\text{A.25})$$

The density is normalized by integrating over all space to obtain the total number of segments of type  $P$

$$\int d\mathbf{r} \rho_p(\mathbf{r}) = n_p \frac{K}{V} \int d\mathbf{r} \int ds \int d\mathbf{R}' \int d\mathbf{R}'' G_p(\mathbf{r}, \mathbf{R}', s) G_p(\mathbf{R}'', \mathbf{r}, N_p - s) = N_p n_p \quad (\text{A.26})$$

The integral over  $\mathbf{r}$  collapses the two Green's functions, the integral over  $s$  yields  $N_p$ , and the normalization constant is found to be

$$\frac{K}{V} = \left( \int d\mathbf{R}' \int d\mathbf{R}'' G_p(\mathbf{R}'', \mathbf{R}', N_p) \right)^{-1} \quad (\text{A.27})$$

The segment densities are, again assuming indistinguishable chains,

$$\rho_p(\mathbf{r}) = \frac{\sum_i^{n_p} \int ds \int d\mathbf{R}' \int d\mathbf{R}'' G_{p_i}(\mathbf{r}, \mathbf{R}', s) G_{p_i}(\mathbf{R}'', \mathbf{r}, N_p - s)}{\int d\mathbf{R}' \int d\mathbf{R}'' G_{p_i}(\mathbf{R}'', \mathbf{R}', N_p)} \quad (\text{A.28})$$

The Poisson–Boltzmann Equation results from applying (A.1) to eq 13 when  $y_i = \psi$ :

$$\frac{\delta F}{\delta \psi(\mathbf{r})} = \frac{\delta}{\delta \psi(\mathbf{r})} \left\{ \int d\mathbf{r} \left[ \frac{1}{2} \beta \epsilon \left| \nabla \psi(\mathbf{r}) \right|^2 + \sum_M \beta e \psi(\mathbf{r}) z_M \rho_M(\mathbf{r}) \right] - \sum_P \sum_i^{n_p} \ln \int d\mathbf{R}_{p_i} \exp\left(-\int ds \Omega_p[\mathbf{R}_p(s)]\right) \right\} \quad (\text{A.29})$$

We again assume indistinguishable chains and let

$$\int d\mathbf{R}_{p_i} \exp\left(-\int ds \Omega_p[\mathbf{R}_p(s)]\right) = \frac{K}{V} \int d\mathbf{r} \Gamma_p(\mathbf{r}) \quad (\text{A.30})$$

Following the same manipulations as for the polymer segment densities, we arrive at

$$\frac{\delta}{\delta \psi(\mathbf{r})} \left\{ \int d\mathbf{r} \left[ \frac{\beta \epsilon}{2} \left( \frac{d\psi(\mathbf{r})}{d\mathbf{r}} \right)^2 + \sum_M \beta e z_M \rho_M(\mathbf{r}) - \sum_P \left( n_p \frac{K}{V} \Gamma_p(\mathbf{r}) - \frac{n_p}{V} \right) \right] \right\} \quad (\text{A.31})$$

Applying the Euler equation gives

$$\frac{d}{d\mathbf{r}} \left( \beta \epsilon \frac{d\psi(\mathbf{r})}{d\mathbf{r}} \right) + \sum_M \beta e z_M \rho_M(\mathbf{r}) - \sum_P n_p \frac{K}{V} \frac{\partial \Gamma_p(\mathbf{r})}{\partial \psi(\mathbf{r})} = 0 \quad (\text{A.32})$$

Here

$$\frac{\partial \Gamma_p(\mathbf{r})}{\partial \psi(\mathbf{r})} = \frac{1}{N_p} \int ds \int d\mathbf{R}' \int d\mathbf{R}'' \frac{\partial}{\partial \psi(\mathbf{r})} (G(\mathbf{r}, \mathbf{R}', s) G(\mathbf{R}'', \mathbf{r}, N_p - s)) \quad (\text{A.33})$$

$$\frac{\partial G(\mathbf{r}, \mathbf{R}', s)}{\partial \psi(\mathbf{r})} = \int_{\mathbf{R}_p(0)=\mathbf{R}}^{\mathbf{R}_p(s)=\mathbf{r}} \delta \mathbf{R}_p(s) \exp\left(-\int_0^s ds' \Omega_p[\mathbf{R}_p(s')]\right) \left( -\int_0^s ds' \frac{\partial \Omega_p[\mathbf{R}_p(s')]}{d\psi(\mathbf{r})} \right) = G(\mathbf{r}, \mathbf{R}', s) (-s \beta e f z_p) \quad (\text{A.34})$$

because  $\partial \Omega_p[\mathbf{R}_p(s)]/\partial \psi(\mathbf{r}) = \beta e f z_p$  when  $\mathbf{R}_p(s) = \mathbf{r}$  for any  $s$  along the chain as required by the functional contour integral, and similarly

$$\frac{\partial G_p(\mathbf{R}'', \mathbf{r}, N_p - s)}{\partial \psi(\mathbf{r})} = G_p(\mathbf{R}'', \mathbf{r}, N_p - s) [-(N_p - s) \beta e f z_p] \quad (\text{A.35})$$

Applying eqs A.33 and A.34 to eq A.32 and simplifying gives the Poisson–Boltzmann equation

$$\nabla^2 \psi(\mathbf{r}) = -\frac{1}{\epsilon} \left( \sum_P f e z_p \rho_p(\mathbf{r}) + \sum_M e z_M \rho_M(\mathbf{r}) \right) \quad (\text{A.36})$$

**Acknowledgment.** The authors are grateful to Professor Sangtae Kim for many insightful discussions and for his support of this work.

**Supporting Information Available:** Additional representative segment density profiles and phase diagrams demonstrating the points discussed in the text. This material is available free of charge via the Internet at <http://pubs.acs.org>.

## References and Notes

- Witten, T. A.; Pincus, P. A. *Macromolecules* **1986**, *19*, 2509–2513.
- Idol, W. K.; Anderson, J. L. *J. Membr. Sci.* **1986**, *28*, 269–286.
- Hesslink, F. T. *J. Colloid Interface Sci.* **1977**, *60*, 448–466.
- Klein, J.; Perahia, D.; Warburg, S. *Nature (London)* **1991**, *352*, 143–145.
- Sidorenko, A.; Minko, S.; Schenk-Meuser, K.; Duschner, H.; Stamm, M. *Langmuir* **1999**, *15*, 8349–8355.
- Netz, R. R.; Schick, M. *Macromolecules* **1998**, *31*, 5105–5122.
- Carignano, M. A.; Szleifer, I. *Macromolecules* **1995**, *28*, 3197–3204.
- Faure, M. C.; Bassereau, P.; Carignano, M. A.; Szleifer, I.; Gallot, Y.; Andelman, D. *Eur. Phys. J. B* **1998**, *3*, 365–375.
- Dolan, A. K.; Edwards, S. F. *Proc. R. Soc. London A* **1975**, *343*, 427–442.
- Dolan, A. K.; Edwards, S. F. *Proc. R. Soc. London A* **1974**, *337*, 509–516.
- Milner, S. T. *Science* **1991**, *251*, 905–914.
- Israels, R.; Leermakers, F. A. M.; Fleer, G. J.; Zhulina, E. B. *Macromolecules* **1994**, *27*, 3249–3261.
- Borisov, O. V.; Zhulina, E. B.; Birsthtein, T. M. *Macromolecules* **1994**, *27*, 4795–4803.
- Csajka, F. S.; Netz, R. R.; Seidel, C.; Joanny, J. F. *Eur. Phys. J. E* **2001**, *4*, 505–513.
- Misra, S.; Mattice, W. L.; Napper, D. H. *Macromolecules* **1994**, *27*, 7090–7098.
- Csajka, F. S.; Seidel, C. *Macromolecules* **2000**, *33*, 2728–2739.
- Pincus, P. *Macromolecules* **1991**, *24*, 2912–2919.
- Kumar, N. A.; Seidel, C. *Macromolecules* **2005**, *38*, 9341–9350.
- Ruhe, J.; Ballauff, M.; Biesalski, M.; Dziezok, P.; Grohn, F.; Johannsmann, D.; Houbenov, N.; Hugenberg, N.; Konradi, R.; Minko, S.; Motornov, M.; Netz, R. R.; Schmidt, M.; Seidel, C.; Stamm, M.; Stephan, T.; Usov, D.; Zhang, H. N. *Adv. Polym. Sci.* **2004**, *165*, 79–150.
- Seidel, C. *Macromolecules* **2003**, *36*, 2536–2543.
- Misra, S.; Varanasi, S.; Varanasi, P. P. *Macromolecules* **1989**, *22*, 4173–4179.
- von Goeler, F.; Muthukumar, M. *Macromolecules* **1995**, *28*, 6608–6617.
- Lyatskaya, Y. V.; Leermakers, F. A. M.; Fleer, G. J.; Zhulina, E. B.; Birshtein, T. M. *Macromolecules* **1995**, *28*, 3562–3569.
- Zhulina, E. B.; Borisov, O. V. *J. Chem. Phys.* **1997**, *107*, 5952–5967.
- Martin, J. I.; Wang, Z. G. *J. Phys. Chem.* **1995**, *99*, 2833–2844.
- Wenning, L.; Muller, M.; Binder, K. *Europhys. Lett.* **2005**, *71*, 639–645.
- Lai, P. Y. *J. Chem. Phys.* **1994**, *100*, 3351–3357.
- Zhulina, E.; Balazs, A. C. *Macromolecules* **1996**, *29*, 2667–2673.
- Muller, M. *Phys. Rev. E* **2002**, *65*, 030802.
- Minko, S.; Muller, M.; Usov, D.; Scholl, A.; Froeck, C.; Stamm, M. *Phys. Rev. Lett.* **2002**, *88*, 035502.
- Marko, J. F.; Witten, T. A. *Phys. Rev. Lett.* **1991**, *66*, 1541–1544.
- Chen, C.; Dan, N.; Dhoot, S.; Tirrell, M.; Mays, J.; Watanabe, H. *Isr. J. Chem.* **1995**, *35*, 41–47.
- Lahann, J.; Mitragotri, S.; Tran, T. N.; Kaido, H.; Sundaram, J.; Choi, I. S.; Hoffer, S.; Somorjai, G. A.; Langer, R. *Science* **2003**, *299*, 371–374.
- Lodge, T. P.; Hillmyer, M. A.; Zhou, Z. L.; Talmon, Y. *Macromolecules* **2004**, *37*, 6680–6682.
- Ludwigs, S.; Boker, A.; Voronov, A.; Rehse, N.; Magerle, R.; Krausch, G. *Nat. Mater.* **2003**, *2*, 744–747.
- Discher, B. M.; Won, Y.-Y.; Ege, D. S.; Lee, J. C. M.; Bates, F. S.; Discher, D. E.; Hammer, D. A. *Science* **1999**, *284*, 1143–1146.
- Borukhov, I.; Andelman, D.; Orland, H. *Eur. Phys. J. B* **1998**, *5*, 869–880.
- Borukhov, I.; Andelman, D.; Orland, H. *Macromolecules* **1998**, *31*, 1665–1671.
- Wang, Q. *Macromolecules* **2005**, *38*, 8911–8922.

- (40) Wang, Q.; Taniguchi, T.; Fredrickson, G. H. *J. Phys. Chem. B* **2004**, *108*, 6733–6744.
- (41) Khokhlov, A. R.; Nyrkova, I. A. *Macromolecules* **1992**, *25*, 1493–1502.
- (42) Doi, M.; Edwards, S. F. *The Theory of Polymer Dynamics*; Oxford University Press: Oxford, UK, 1986.
- (43) Holst, M. J. The Poisson–Boltzmann Equation: Analysis and Multilevel Numerical Solution. Ph.D. Thesis, Univeristy of Illinois, Urbana–Champaign, IL, 1994.
- (44) Wilde, D. J. *Optimum Seeking Methods*; Prentice Hall: Englewood Cliffs, NJ, 1964.
- (45) Ionov, L.; Houbenov, N.; Sidorenko, A.; Stamm, M.; Luzinov, I.; Minko, S. *Langmuir* **2004**, *20*, 9916–9919.
- (46) Arfken, G. B.; Weber, H. J. *Mathematical Methods for Physicists*, 5th ed.; Academic Press: San Diego, 2000.

MA0608370

## Errata

- p. 7759 left, line 23 from top (4<sup>th</sup> line in eq 13): “[d $\mathbf{R}_{P_i}$ ” should be “[D $\mathbf{R}_{P_i}$ ”.
- p. 7762 left, line 9 from bottom: “ $b^3 \gg 343 \text{ \AA}^3$ ” should be “ $b^3 \approx 343 \text{ \AA}^3$ ”.
- p. 7763 left, line 10 from bottom: “ $f_c \gg 0.18$ ” should be “ $f_c \approx 0.18$ ”.
- p. 7764 left, line 18 from bottom: “ $C_{M,c} \gg 150 \text{ mM}$ ” should be “ $C_{M,c} \approx 150 \text{ mM}$ ”.
- p. 7766 right, line 7 from top: “ $\exp(x) \approx (1 + \{x\}/\{n\})^n$ ” should be “ $e^x \approx (1 + x/n)^n$ ”.

Supporting Information for

**Self-Consistent Field (SCF) Analysis of Mixed Polyelectrolyte and Neutral Polymer  
Brushes**

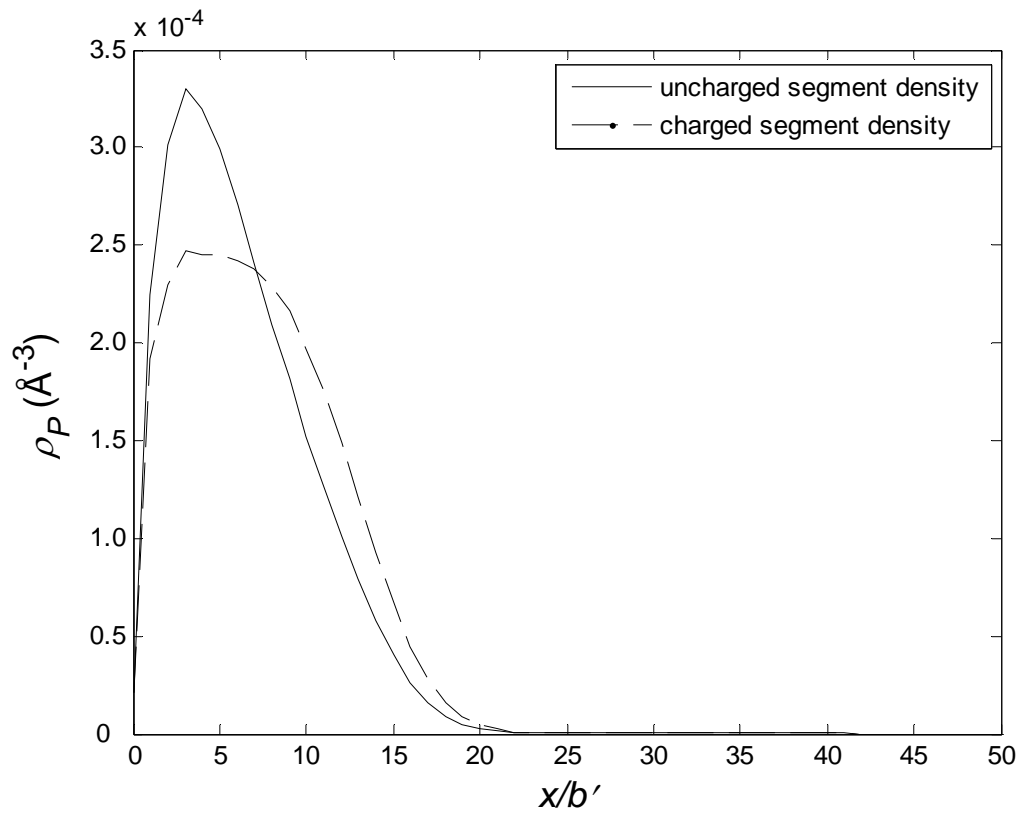
Kevin N. Witte, and You-Yeon Won \*

*School of Chemical Engineering, Purdue University, West Lafayette, Indiana 47907*

---

\* [yywon@ecn.purdue.edu](mailto:yywon@ecn.purdue.edu)

(a)



(b)

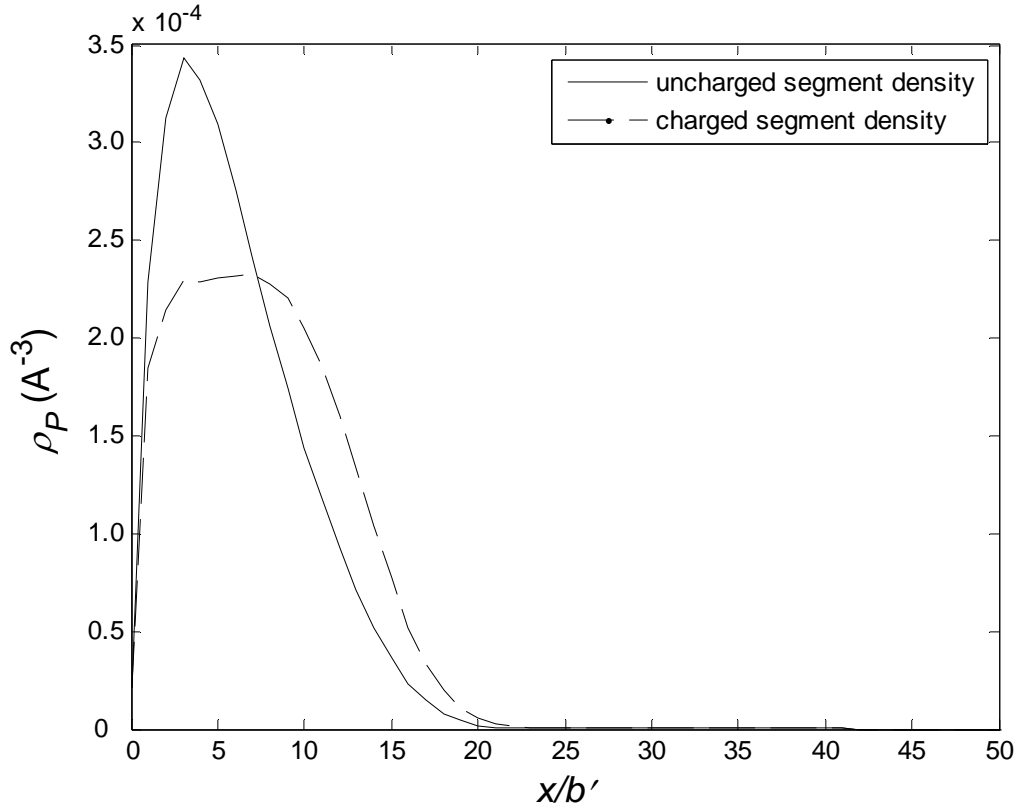


**Figure S1.** Plots demonstrating the inability to use the segment density profiles as a means for determining macroscopic phase separation of mixed polyelectrolyte/neutral polymer brushes. (a) Representative segment density  $\rho_P$  profile inside the spinodal envelope shown in Figure 4 (spontaneous macroscopic phase separation), assuming fixed grafting endpoints, as a function of reduced distance from the grafting surface  $x/b'$  for chain length  $N = 49$  with Kuhn length  $b = 7 \text{ \AA}$ , charge fraction on the polyelectrolyte chains  $f = 0.16$ , grafting density  $\sigma = 0.0005 \text{ \AA}^{-2}$ , excluded volume interactions  $v_{AA} = 125 \text{ \AA}^3$ ,  $v_{AC} = 215 \text{ \AA}^3$ ,  $v_{CC} = 100 \text{ \AA}^3$ , bulk salt concentration  $c_M = 150 \text{ mM}$ , and composition  $x_C = 0.5$ . (b) Representative segment density  $\rho_P$  profile outside the two phase envelope shown in Figure 4 (no macroscopic phase separation) as a function of reduced distance from the grafting surface  $x/b'$  for charge fraction on the polyelectrolyte chains  $f = 0.19$  with all the other parameters the same as above.

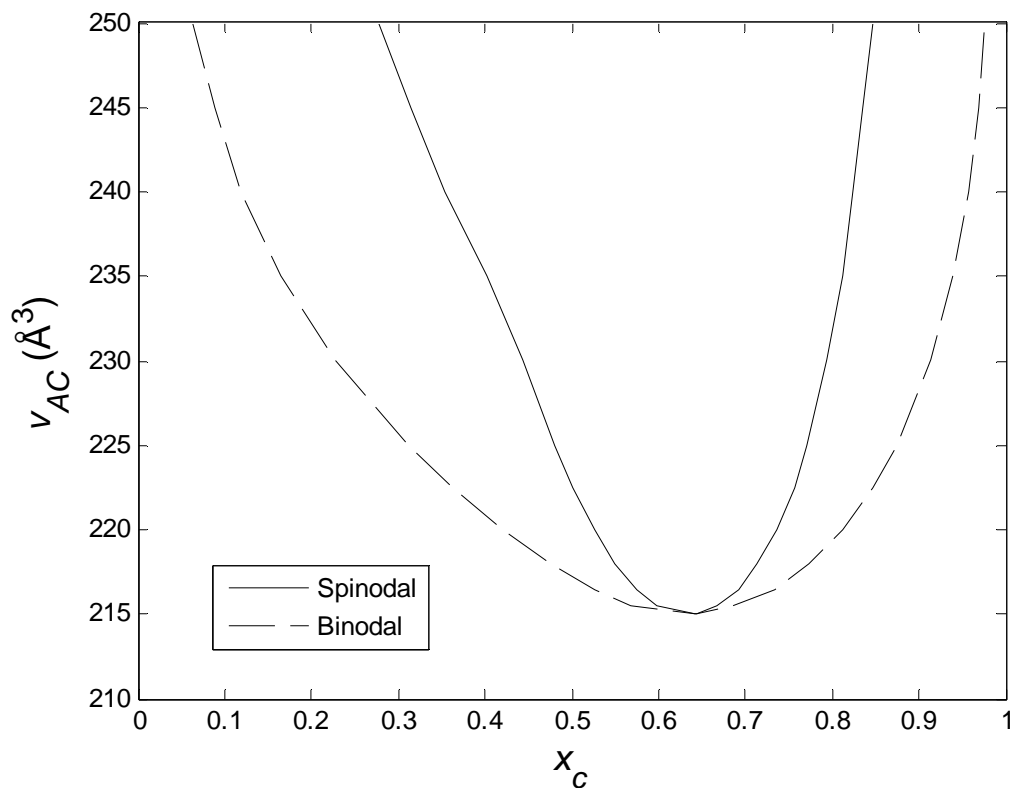


**Figure S2.** Phase diagram demonstrating decreasing miscibility with increasing neutral polymer and charged polymer excluded volume cross-interaction parameter  $v_{AC}$  as a function of composition  $x_C$  for  $N = 49$  with Kuhn length  $b = 7 \text{ \AA}$ , charge fraction on the polyelectrolyte chains  $f = 0.18$ , grafting density  $\sigma = 0.0005 \text{ \AA}^{-2}$ , excluded volume interactions  $v_{AA} = 125 \text{ \AA}^3$ ,  $v_{CC} = 100 \text{ \AA}^3$ , and bulk salt concentration  $c_M = 150 \text{ mM}$ .

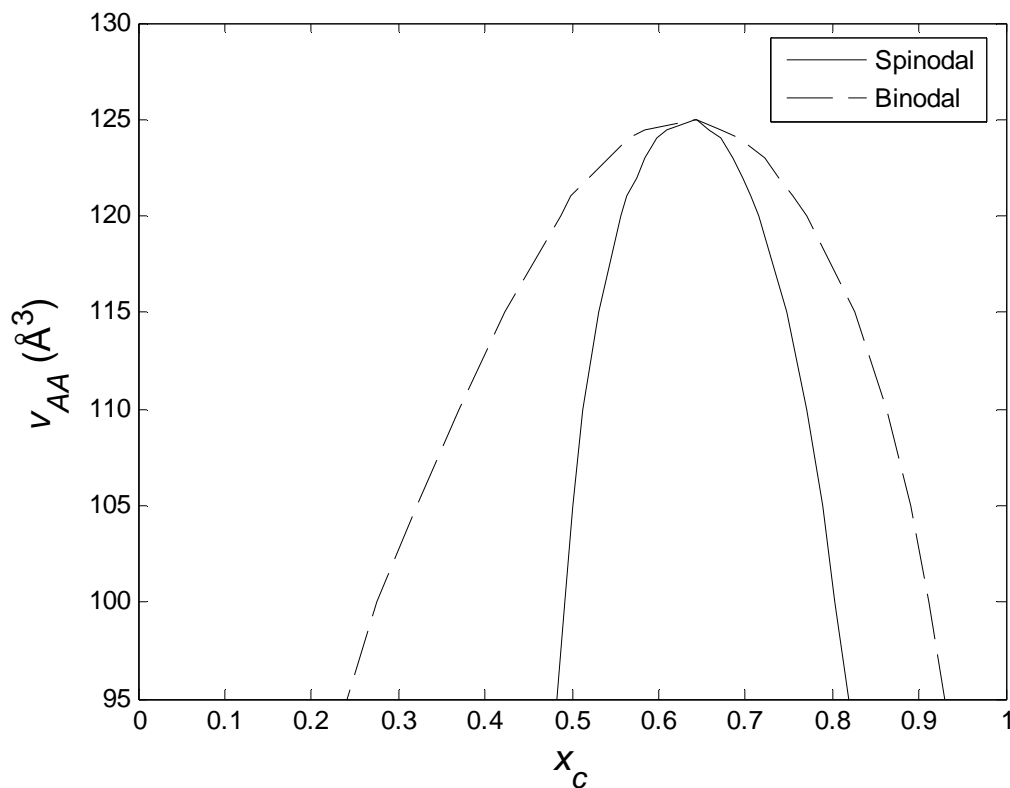


**Figure S3.** Phase diagram demonstrating increasing miscibility with increasing neutral polymer excluded volume self-interaction parameter  $v_{AA}$  as a function of composition  $x_C$  for  $N = 49$  with Kuhn length  $b = 7 \text{ \AA}$ , charge fraction on the polyelectrolyte chains  $f = 0.18$ , grafting density  $\sigma = 0.0005 \text{ \AA}^{-2}$ , excluded volume interactions  $v_{AC} = 215 \text{ \AA}^3$ ,  $v_{CC} = 100 \text{ \AA}^3$ , and bulk salt concentration  $c_M = 150 \text{ mM}$ .

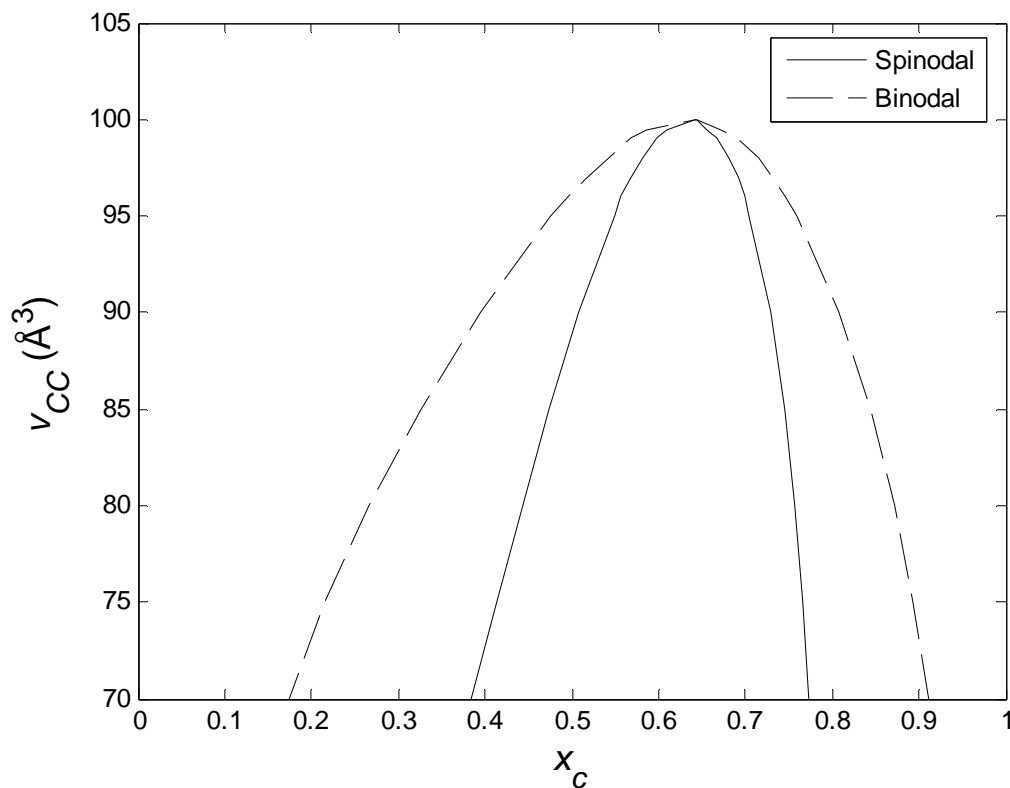


**Figure S4.** Phase diagram demonstrating increasing miscibility with increasing charged polymer excluded volume self-interaction parameter  $v_{CC}$  as a function of composition  $x_C$  for  $N = 49$  with Kuhn length  $b = 7 \text{ Å}$ , charge fraction on the polyelectrolyte chains  $f = 0.18$ , grafting density  $\sigma = 0.0005 \text{ Å}^{-2}$ , excluded volume interactions  $v_{AA} = 125 \text{ Å}^3$ ,  $v_{AC} = 215 \text{ Å}^3$ , and bulk salt concentration  $c_M = 150 \text{ mM}$ .

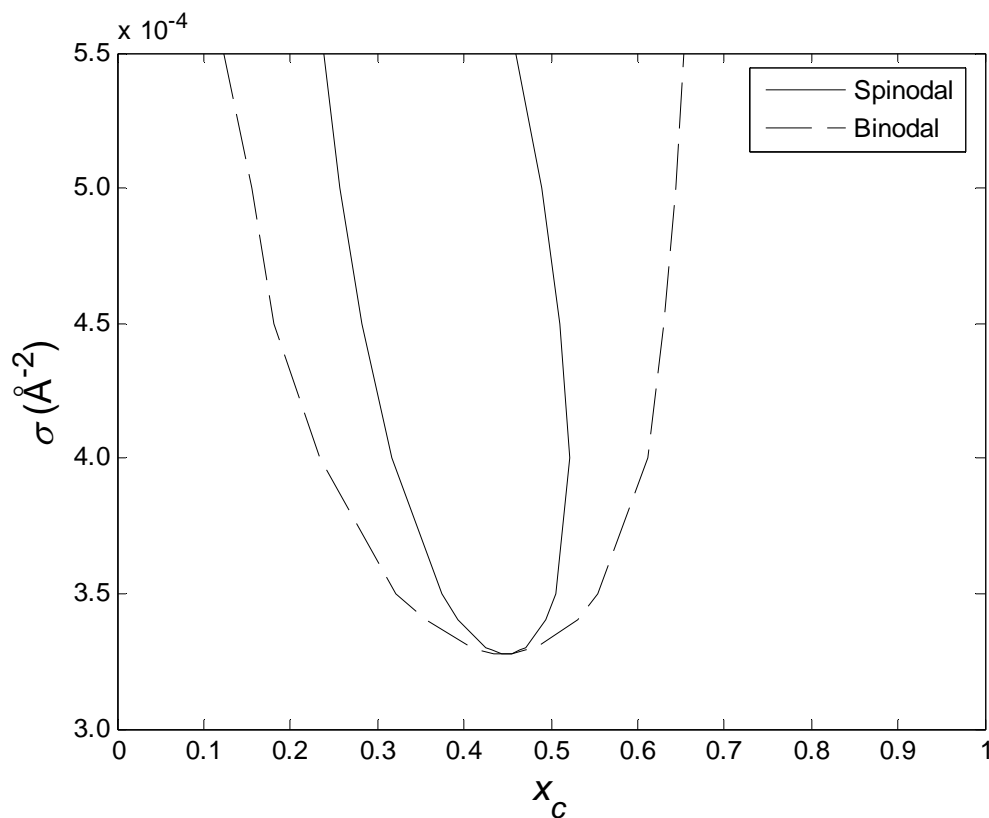


**Figure S5.** Phase diagram demonstrating the switching of asymmetry (as compared to Figure 6 which is discussed in Section 3.3 of the main paper) due to variation in the excluded volume parameters as functions of grafting density  $\sigma$  and composition  $x_C$  for chain length  $N = 49$  with Kuhn length  $b = 7 \text{ \AA}$ , charge fraction on the polyelectrolyte chains  $f = 0.18$ , excluded volume interactions  $v_{AA} = 200 \text{ \AA}^3$ ,  $v_{AC} = 215 \text{ \AA}^3$ ,  $v_{CC} = 10 \text{ \AA}^3$ , and bulk salt concentration  $c_M = 150 \text{ mM}$ .